PHILOSOPHICAL TRANSACTIONS OF THE ROYAL SOCIETY A

rsta.royalsocietypublishing.org

Research

Cite this article: John EH, Pearson PN, Coxall HK, Birch H, Wade BS, Foster GL. 2013 Warm ocean processes and carbon cycling in the Eocene. Phil Trans R Soc A 371: 20130099. http://dx.doi.org/10.1098/rsta.2013.0099

One contribution of 11 to a Discussion Meeting Issue 'Warm climates of the past—a lesson for the future?'.

Subject Areas:
biogeochemistry, climatology, geochemistry, geology, palaeontology

Keywords:
Eocene, planktonic foraminifera, biological pump, stable isotopes, carbon cycling temperature

Author for correspondence:
Eleanor H. John
e-mail: johneh@cf.ac.uk

Royal Society Publishing
Informing the science of the future

Warm ocean processes and carbon cycling in the Eocene

Eleanor H. John[1], Paul N. Pearson[1], Helen K. Coxall[2], Heather Birch[1], Bridget S. Wade[3] and Gavin L. Foster[4]

[1]School of Earth and Ocean Sciences, Cardiff University, Park Place, Cardiff CF10 3AT, UK
[2]Department of Geological Sciences, Stockholm University, Svante Arrhenius väg 8, 106 91 Stockholm, Sweden
[3]School of Earth and Environment, University of Leeds, Woodhouse Lane, Leeds LS2 9JT, UK
[4]Ocean and Earth Science, National Oceanography Centre Southampton, University of Southampton, European Way, Southampton SO14 3ZH, UK

Sea surface and subsurface temperatures over large parts of the ocean during the Eocene epoch (55.5–33.7 Ma) exceeded modern values by several degrees, which must have affected a number of oceanic processes. Here, we focus on the effect of elevated water column temperatures on the efficiency of the biological pump, particularly in relation to carbon and nutrient cycling. We use stable isotope values from exceptionally well-preserved planktonic foraminiferal calcite from Tanzania and Mexico to reconstruct vertical carbon isotope gradients in the upper water column, exploiting the fact that individual species lived and calcified at different depths. The oxygen isotope ratios of different species' tests are used to estimate the temperature of calcification, which we converted to absolute depths using Eocene temperature profiles generated by general circulation models. This approach, along with potential pitfalls, is illustrated using data from modern core-top assemblages from the same area. Our results indicate that, during the Early and Middle Eocene, carbon isotope gradients were steeper (and larger) through the upper thermocline than in the modern ocean. This is consistent with a shallower average depth of organic matter remineralization and supports previously proposed hypotheses that invoke high metabolic rates in a warm Eocene ocean, leading to more efficient recycling of organic matter and reduced burial rates of organic carbon.

1. Introduction

There are many concerns about the impact of anthropogenic global warming on the oceans, including changes to thermal structure, circulation patterns, oxygenation and pH [1,2]. The effect of a warmer ocean on the efficiency of the marine biological pump has also been emphasized, due to the fact that respiration rates in remineralizing microbes are temperature-dependent [3–6]. This may be important for understanding the response of the carbon cycle to current warming trends on short and geological time scales. To predict the effects of warming, these processes can be modelled [4]; another approach is to examine them for warm climate states in the past.

During the Eocene epoch (55.5–33.7 Ma), global mean temperatures were undoubtedly higher than today, and the poles are thought to have been largely ice-free. Evidence for Eocene warmth in marine and terrestrial realms is diverse and includes records of the distribution of biological taxa (e.g. the presence of cold-blooded animals and frost-intolerant plant species at high latitudes [7–9]) and analysis of leaf morphology [10]. The oxygen stable isotope ratio ($\delta^{18}O$) of deep-sea benthic foraminifera [11–14] shows that bottom waters probably exceeded 10–12°C in the Early Eocene, cooling to 5°C by the end of the epoch [13,14]. This trend was interrupted by intervals of relative stability or transient warming events, such as at the Middle Eocene Climatic Optimum [15,16]. Sea surface temperatures reconstructed using the $\delta^{18}O$ values of well-preserved planktonic foraminifera [17] and organic proxies also indicate warmer temperatures than the modern throughout the Eocene, particularly at high latitudes [18,19]. Tropical temperatures remained relatively warm and roughly constant during the Eocene, which suggests that the cooling occurred mainly at high latitudes [17,18]. Although there is some quantitative disagreement between proxies, the general implication that large areas of the open ocean were warmer than the modern for most of the Eocene is sound, and it is unlikely that global Eocene temperatures have been exceeded since.

Elevated seawater temperatures could have affected the state of the Earth system in many ways, for example causing changes in ocean circulation, evaporation patterns, cloud formation, latent heat transfer to the atmosphere and increased storminess over large areas [20,21]. Higher ocean temperatures may also have affected the biological pump, that is, the biologically mediated transport of organic carbon out of the surface ocean to the ocean interior before it is remineralized back to CO_2 [22] (figure 1). Bacterial respiration is the main way that sinking organic matter is decomposed and carbon and nutrients that were fixed near the surface through photosynthesis are recycled at depth. Because the metabolic rates of these remineralizing bacteria are temperature-dependent, elevated ocean temperatures may result in more efficient recycling of carbon and nutrients higher in the water column, thus affecting the amount of sinking carbon that reaches the deep sea and seafloor sediments. Because microbial respiration produces CO_2, this would also alter the distribution of dissolved inorganic carbon (DIC) in the water column as well as potentially affecting atmospheric CO_2. If the oceans were indeed globally warmer during the Eocene, these effects may also have been global, and therefore need to be addressed if we are to understand global carbon cycling. This was emphasized by Olivarez Lyle & Lyle [24], who postulated that higher Eocene temperatures and enhanced remineralization rates were responsible for reduced organic carbon burial rates in the deep sea. Such effects may have been an important feedback on the global climate throughout the Phanerozoic [4,25].

Bacterial remineralization of organic matter also results in the redistribution of carbon isotopes in the water column: photosynthetic carbon fixation in the photic zone preferentially removes ^{12}C, leaving the remaining DIC pool with elevated $\delta^{13}C_{DIC}$ values; upon sinking, microbes respire this organic matter and return the isotopically light carbon to the DIC pool. This is reflected in a general decrease in $\delta^{13}C_{DIC}$ values with depth in the upper part of the water column (figure 1). Potentially, depth-stratified planktonic foraminifera can also record this process of organic matter remineralization as a decrease in the $\delta^{13}C$ of their test calcite with increased water depth habitat [26]. The actual shape of $\delta^{13}C_{DIC}$–depth profiles is highly variable worldwide, but among the main controls on the shape of the profile are the depth and efficiency of remineralization processes in the water column.

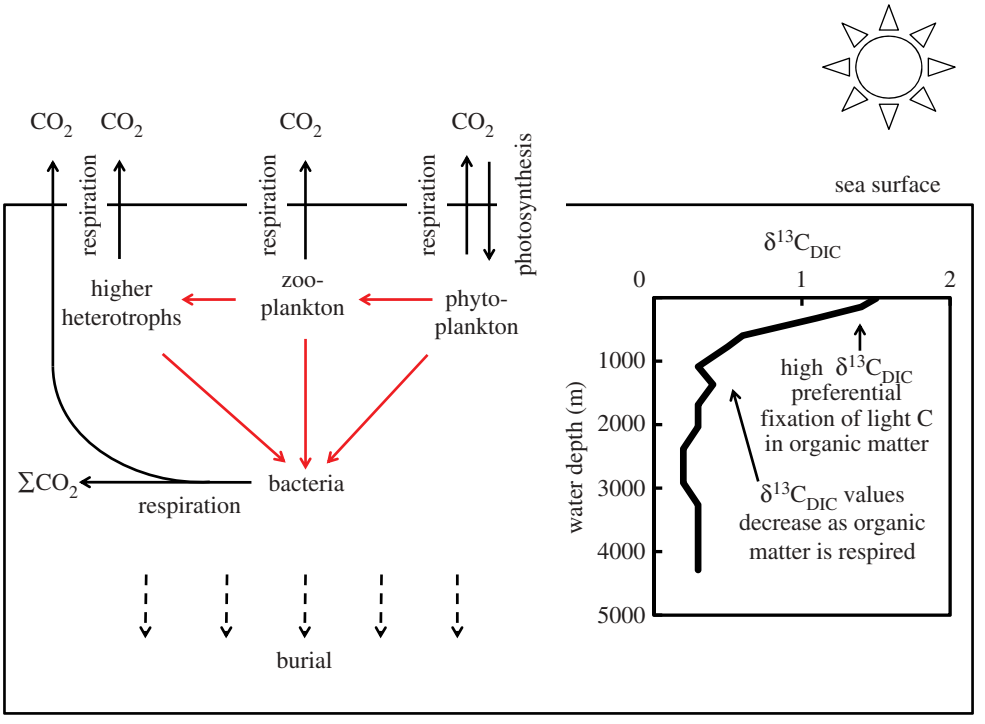

Figure 1. Schematic cartoon of the modern biological pump showing production of organic matter, its consumption by higher organisms and the respiration of CO_2. The profile on the right-hand side shows a $\delta^{13}C_{DIC}$ profile from a site offshore of modern Tanzania (data taken from site 425 of Kroopnick [23]) to illustrate the typical decrease in $\delta^{13}C_{DIC}$ with depth due to preferential fixation of isotopically light carbon in the surface ocean during photosynthesis and the subsequent return of this light carbon as sinking organic matter is respired by microbes.

In this contribution, we investigate these effects by using assemblages of exceptionally well-preserved planktonic foraminifera from the Eocene of Tanzania and Mexico to reconstruct the vertical gradient of stable carbon isotope ratios in DIC ($\delta^{13}C_{DIC}$) in the water column for various time slices throughout the epoch. This has not previously been carried out using foraminifera that have not been subject to the micrometre-scale recrystallization that is common in deep-sea carbonates; this is important because such recrystallization can dampen surface-to-deep $\delta^{13}C_{DIC}$ offsets. We use these profiles to decipher information about water column processes, including the efficiency of the biological pump during the Eocene in comparison with today.

2. The metabolic hypothesis and the Q_{10} relationship

There is a rich literature on the effects of temperature on biological activity. Arrhenius [27] described the exponential increase in inorganic reaction rates with temperature in terms of 'Q_{10}', the fractional increase in reaction rate for every 10°C increase in temperature. It has long been known that metabolic rates in ectothermic organisms also follow the Q_{10} pattern and show a very approximate doubling per 10°C increase (i.e. $Q_{10} \approx 2.0$). This includes marine and terrestrial microbial decomposers, whose measured Q_{10} activities lie between approximately 2 and 4 [28–32]. The Q_{10} pattern can also be used to describe the temperature dependence of metabolic rates in a more diverse range of life forms, from unicellular ectotherms to large endothermic mammals, with other factors such as body size playing important additional roles. These relationships have been expanded to describe entire complex ecosystems in terms of the role that temperature plays in regulating an ecosystem's 'metabolism' [33–35].

Theory predicts that metabolic rates in all oceanic planktonic communities should be strongly dependent on temperature [33–37]. Importantly, while both rates of respiration and rates of photosynthesis should increase with increasing temperature, the effect of temperature is stronger in the former [37], leading to an increasing dominance of heterotrophic activity in warmer waters. This has been demonstrated in the modern oceans [3,6,38]. Based on a large database of 1156 volumetric estimates of oceanic planktonic metabolism and temperature measurements, Regaudie-de-Gioux & Duarte [6] demonstrated strong relationships between both gross primary production and community respiration rates and temperature, and found average Q_{10} values for the whole ocean of 1.56 for gross primary production and 2.52 for community respiration. The values were comparable in the two hemispheres, but were different between ocean basins and between seasons, reflecting changes in planktonic community structure. The positive relationship between temperature and the ratio of respiration/primary production appears to be strong below 20–21°C [3,6], with a weaker relationship at higher temperatures due to an overall dominance of heterotrophs [3]. Feedbacks within the global carbon cycle are likely, because areas of net heterotrophy represent sources of CO_2 to the atmosphere provided there is an allochthonous source of food for the microbes [38].

These relationships also have a bearing on the biological pump, as enhanced rates of organic carbon remineralization could reduce the amount of organic carbon reaching the deep ocean and the seafloor. Laws *et al*. [3] used a complex pelagic food web model to investigate controls on modern export production, including ecological interactions, controls on the metabolic rates of different organisms and other dynamic processes. They concluded that temperature variations could account for more than 80% of the variance in their modelled export production. Several studies have used modelling results to emphasize the effect of temperature-dependent remineralization on the strength of the organic carbon pump, atmospheric CO_2 and nutrient distribution in the ocean, primarily on glacial–interglacial time scales for which we have a wealth of data to cross-check with the model. Matsumoto [4] used results from an intermediate-complexity climate model to account for around one-third of the changes in CO_2 between Plio-Pleistocene glacials and interglacials by invoking suppressed microbial activity and a stronger organic pump strength during colder glacials. This led to a lower relative export rate of $CaCO_3$ versus C_{org} to the deep seafloor (i.e. a lower 'rain ratio'). From a comprehensive map of rain ratios and their high-resolution regional ocean ecosystem model, Matsumoto [4] proposed that today's rain ratios are controlled, at least in part, by temperature through both enhanced remineralization of organic matter and temperature dependence of community composition. Chikamoto *et al*.'s [39] model simulations include temperature-dependent remineralization rates and they came to similar conclusions about the importance of temperature in controlling export production.

It seems clear that the effects of temperature on the biological pump could have strong implications for our understanding of controls on carbon cycling in ancient greenhouse worlds. However, these ideas have been little discussed in relation to the warm Eocene oceans or other warm intervals of the past. Gu *et al*. [40] proposed that a warmer ocean would increase rates of methanogenesis in seafloor sediments, thus providing a source for the isotopically light carbon released during Eocene hyperthermals. However, a warmer ocean would presumably also affect rates of aerobic respiration of sinking organic matter. Olivarez Lyle & Lyle [24] suggested that the discrepancy between percentages of biogenic Ba (an indicator of primary productivity) and organic matter preserved in Early Eocene sediments from the equatorial Pacific could be explained through increases in microbial respiration rates in a warmer ocean and a subsequent reduction in the burial rate of organic carbon. They also suggest that increased DIC concentrations in the water column (caused by enhanced biogenic production of CO_2) relative to alkalinity inputs from weathering on land and subsequent shoaling of the carbonate compensation depth (CCD) would lead to reduced inorganic carbon burial. This relatively simple model involving positive feedbacks was suggested as a mechanism for maintaining high pCO_2 levels in greenhouse worlds and inversely low greenhouse gas concentrations in icehouse worlds [24] (see also Stanley [25]).

There are various complications with these ideas. For example, it is difficult to conceive how elevated pCO_2 levels can be maintained by these processes in the light of the tight inorganic feedbacks that mediate atmospheric CO_2 change, such as variations in silicate weathering [41]. It has also been suggested that calcium carbonate, the dominant test mineralogy among Eocene plankton, is a more effective ballasting agent than biogenic opal, which dominates planktonic communities today, more rapidly transporting organic matter to the seafloor for subsequent burial [42–44], although recent work suggests that the importance of mineral ballasting may have been overestimated [45]. The effects on the distribution of oxygen minimum zones (OMZs) in the oceans should also be considered (oxygen is consumed by microbial respiration), although at present the distribution of OMZs is mainly controlled by large-scale circulation patterns. Despite these considerations, it is clear that there were probably radical differences between the ways in which the marine biological pump operated in the warm Eocene compared with today; this study represents an attempt to detect such differences using the stable isotope record of foraminiferal calcite.

3. The Tanzania foraminifer stable isotope record

Foraminifera are unicellular protists that are abundant in oceanic environments. Some species are benthic; others live as plankton, with habitats distributed through the upper part of the water column [46]. Foraminifera secrete 'tests' (shells) of calcium carbonate that accumulate on the seafloor after death and can be a major component of pelagic sediments. A suite of geochemical proxies can be extracted from foraminifer tests to provide information about the water in which they calcified; here, we focus on a combination of oxygen and carbon isotope ratios.

The oxygen isotope ratio of calcite is dependent, in part, on the temperature of the water in which it calcified: $\delta^{18}O$ values increase with water depth in accordance with the accompanying decrease in temperature [12,47]. The carbon isotope ratio of calcite depends largely on that of the bicarbonate ion (HCO_3^-) from which it precipitated [48], which, in turn, reflects air–sea exchange processes in the surface ocean and biological activity. There is a nonlinear relationship between $\delta^{13}C_{DIC}$ and depth because of the photosynthetic fixation of isotopically light carbon in the surface ocean and its subsequent remineralization at depth (figure 1). However, stable isotope ratios in foraminiferal tests are affected by other factors, which mean that calcification does not occur in isotopic equilibrium with ambient seawater (see below). Insights into such disequilibrium effects in modern assemblages were made by Birch *et al*. [49] (§4) and their observations are applied in this study.

Here, we use stable isotope ratios of planktonic foraminifera from Eocene hemipelagic sediments of Tanzania, as published as supplementary information to Pearson *et al*. [17] and in Wade & Pearson [50], and from an Eocene shale of eastern Mexico (the Guayabal Formation), as published in Pearson *et al*. [51]. The significance of the carbon isotope data has not previously been discussed. These Tanzanian and Mexican data are particularly valuable, as they are derived from exceptionally well-preserved assemblages with no evidence of micrometre-scale recrystallization [17,51] (see also [52]). This is important, because such diagenesis can have a large effect on the stable isotope composition of foraminiferal tests, including $\delta^{13}C$ [17,53], despite claims to the contrary [54]. The Tanzanian assemblages represent those typical of open ocean conditions, complete with deep-dwelling forms, and were deposited in an upper bathyal environment [55,56]. The single Mexican dataset also represents a typical open ocean assemblage. The ages of the core samples are determined by foraminiferal and nanofossil biostratigraphy [17,51]. Recent advances in Eocene biostratigraphy have resulted in significant changes in the ages of several bioevents in the earliest Middle Eocene; we have therefore updated the age of each sample in comparison with the previous publications as per Wade *et al*. [57]. The Tanzanian samples range in age between 54.90 and 33.75 Ma and the single Mexican sample is dated at 42.05 ± 1.55 Ma. During these times, relatively warm conditions prevailed in Tanzania and eastern Mexico, with reconstructed sea surface temperatures in the range 30–34.5°C [17,50,51] (compared with 27–30°C for the modern [49]).

4. Multi-species and dissolved inorganic carbon in the modern

In this section, we describe the approach of reconstructing water column $\delta^{13}C_{DIC}$ gradients using stable isotope data from foraminiferal assemblages by summarizing data from a modern core-top assemblage from offshore Tanzania, as studied by Birch *et al*. [49]. Although limited to one location, this study is useful in presenting data from a wide range of planktonic foraminifera shell sizes (80–800 µm, taxon-dependent) for each species investigated. The results provide new insights into foraminiferal test $\delta^{13}C$ variability that refine our ability to recognize several vital effects, including disequilibrium effects, in geochemical data from fossil assemblages.

Birch *et al*. [49] measured $\delta^{13}C$ and $\delta^{18}O$ values in 12 species of planktonic foraminifera from a single core-top sample. Using a series of sieves with increasing mesh size, a total of 60 species-specific, size-controlled splits were separated (each consisting of multiple shells), so that the effects of size and species on the isotope ratios could be investigated in detail. Figure 2 shows the $\delta^{13}C$ and $\delta^{18}O$ data from the multi-species size fraction splits plotted against each other. The variability along the $\delta^{18}O$ axis primarily reflects the depth of calcification (with warmer waters, i.e. lower $\delta^{18}O$ values, near the surface) and seasonal variations. Birch *et al*. first used their $\delta^{18}O$ values to determine temperature using the equation of Erez & Luz [59] and then overlaid this temperature on the measured water column temperature profile to estimate absolute depth of calcification. They used water column $\delta^{13}C_{DIC}$ measurements from a range of locations near their study site to determine the approximate values that would result if the foraminifer tests had calcified in approximate isotopic equilibrium with ambient seawater temperature and $\delta^{13}C_{DIC}$ under conditions of 'normal' water column structure. Measurements from a range of settings (about 2500 to more than 5000 m water depth) within approximately 800 km of their study site [60] yielded similar-shaped profiles and absolute values, and a compilation of these values is represented by a grey band in figure 2 (see Birch *et al*. [49] for details). The width of the band was also intended to account for seasonal effects. The fact that Birch *et al*.'s data do not all fall close to this band or any single line in figure 2 implies that other factors are influencing the $\delta^{13}C$ values. The position of the data with respect to the typical 'equilibrium line' helps us demonstrate four main types of effect (illustrated in figure 2):

(i) The metabolic fractionation effect. Foraminifera that are smaller than the 212 µm sieve size (either adults of relatively small species or the juvenile stages of larger species) tend to have $\delta^{13}C$ values that are more negative than ambient seawater—the offset being greatest for the smallest size fractions [61]. This is thought to be due to the incorporation of a fraction of isotopically light carbon from organic matter that has previously been respired by the foraminifer itself. The fraction of metabolic carbon in the foraminifer test decreases as the foraminifer grows, as the rate of metabolic activity decreases and exchange of carbon with ambient seawater improves [61–66].

(ii) The photosynthetic fractionation effect. Many species of near-surface-dwelling planktonic foraminifera have a symbiotic relationship with photosynthesizing algae, mainly dinoflagellates. These algae preferentially remove ^{12}C during photosynthesis, leaving the remaining seawater isotopically heavy with respect to ambient DIC; such locally elevated $\delta^{13}C$ values may then be recorded by the foraminifera [26,67–72]. As foraminifera grow to larger sizes, so the cloud of algae surrounding the foraminifer test increases, and the photosynthetic effect is increasingly pronounced in successive size fractions. This becomes particularly marked in the tests of symbiotic species over approximately 355 µm diameter [49].

(iii) The pH fractionation effect. A few species are adapted to deepwater habitats close to the oxygen minimum zone where the pH is reduced. Such species may have $\delta^{13}C$ values that show a positive offset from equilibrium values, and it has been postulated that this is due to pH-dependent fractionation effects [48,49,73].

(iv) The seasonal upwelling effect. Certain species, including *Globigerina bulloides* and the small species *Globigerinita glutinata*, as discussed in the study of Birch *et al*. [49], together

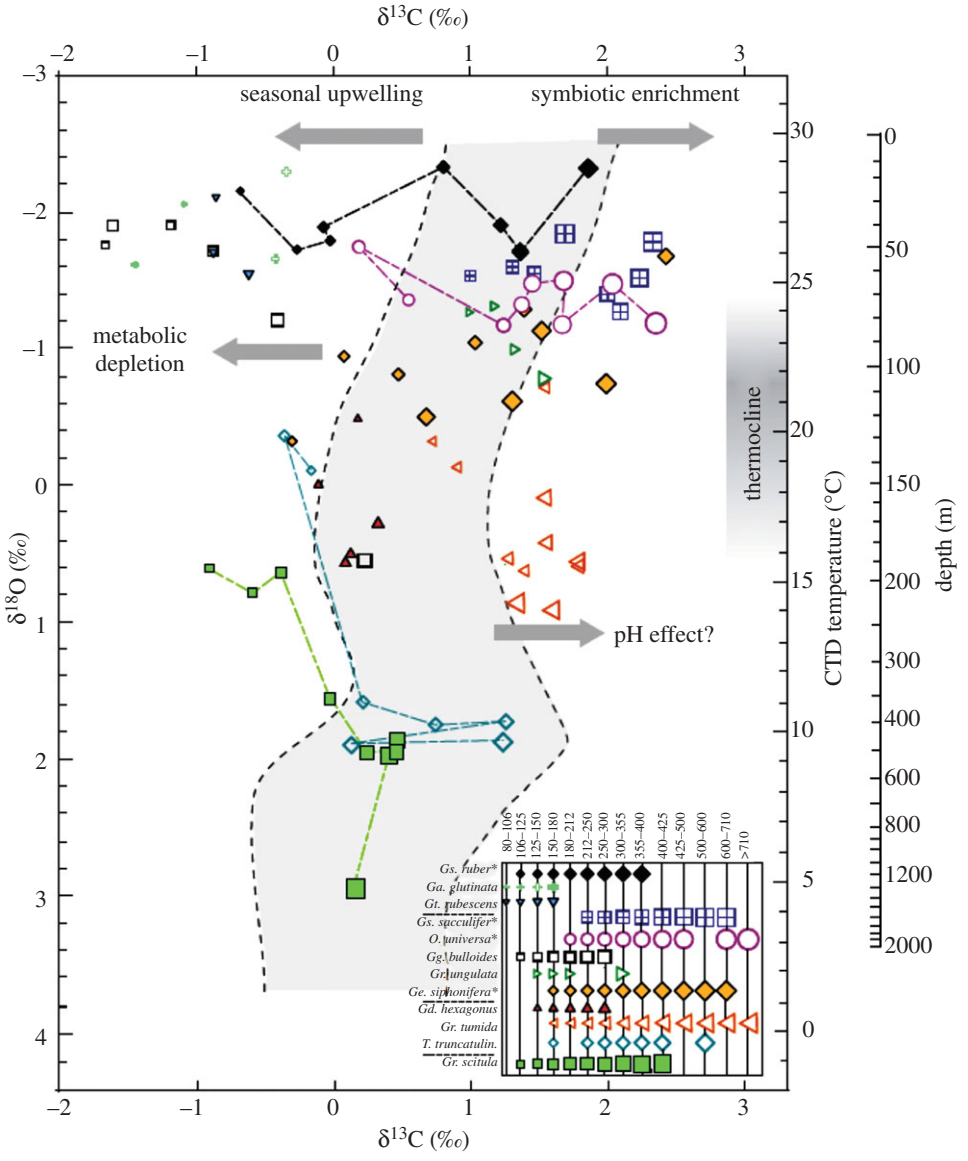

Figure 2. Multi-species $\delta^{18}O$ and $\delta^{13}C$ cross-plot for a modern core-top foraminifera assemblage from approximately 200 km offshore of Tanzania (latitude 8°51.5538′ S, longitude 41°26.4102′ E) at a water depth of 3006 m [58]. (Adapted from fig. 7 of Birch *et al*. [49] (full caption given therein).) The site is oligotrophic, as shown by the conductivity temperature depth (CTD) probe data and the assemblage composition, which is dominated by typical oligotrophic species with only a very minor fraction of species that represent seasonal upwelling (e.g. *Globigerinita glutinata*). Planktonic foraminifera $\delta^{18}O$ values were converted to temperature according to the relationship of Erez & Luz [59] and using a modern seawater $\delta^{18}O_w$ value of 0.47‰. The grey band represents a composite of water column $\delta^{13}C_{DIC}$ measurements taken from seven sites within approximately 800 km of their study site (from World Ocean Database) and incorporating a ±0.5‰ window to account for seasonal variations. Data points falling outside of this band are thought to represent calcification out of isotopic equilibrium with DIC or by foraminifera that calcified during episodes of seasonal upwelling (i.e. *Gg. bulloides* and *Ga. glutinata*). For species with obligate symbionts (asterisk), the largest individuals have $\delta^{13}C$ values up to 1.0‰ higher than the equilibrium envelope owing to photosynthetic activity by symbiotic algae. The smallest individuals of most species have $\delta^{13}C$ values that are 0.2–2.0‰ lower than the envelope because of size-related metabolic effects. The $\delta^{13}C$ measured in mid-sized shells (in the approx. 212–355 μm size fraction) in fossil assemblages should therefore provide the closest approximation of $\delta^{13}C_{DIC}$. *Gs.*, *Globigerinoides*; *Ga.*, *Globigerinita*; *Gt., Globoturborotalita; O., Orbulina*; *Gg., Globigerina; Gr., Globorotalia; Ge., Globigerinella; Gd., Globorotaloides; T., Truncorotalia*.

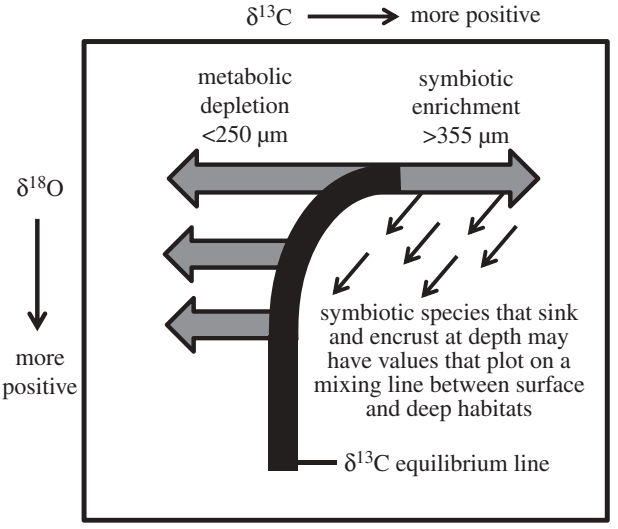

Figure 3. Cartoon showing how data points plotting in different fields of the $\delta^{18}O$ and $\delta^{13}C$ cross-plots can be interpreted after Pearson & Wade [66].

with *Neogloboquadrina dutertrei* [74–76], are indicative of more productive tropical surface conditions linked to seasonal upwelling [75–77]. The $\delta^{13}C$ value of such species' tests is therefore more similar to that of deeper-dwelling species because they record the isotopic chemistry of cool, ^{12}C-rich, upwelling deepwaters. It should be noted, however, that these species only make up a small proportion of those presented in figure 2, which otherwise resembles an oligotrophic assemblage [49].

To counteract these effects when reconstructing the water column $\delta^{13}C_{DIC}$ gradient, Birch *et al*. [49] recommend that surface mixed-layer $\delta^{13}C$ values are best estimated using foraminifera in the middle of their size range, i.e. 212–355 µm (figure 2), and if deep-dwelling species show unexpected scatter in their $\delta^{13}C$ values, then ambient $\delta^{13}C$ is best estimated using the more negative values. From figure 2, it can be seen that these relatively simple rules apply reasonably well to the modern dataset. Some scatter is always expected owing to seasonal and interannual variability in water column structure and chemistry at any given site. Another complication is that some species might change their position in the water column during their life cycle; in particular, some surface-dwelling symbiotic forms sink in their final life stages to reproduce, forming a crust of gametogenic calcite [67]. The measured stable isotope values in adult size fractions of such species will plot on a mixing line between the two depth habitats (figures 2 and 3). This effect is not obvious in the modern data of Birch *et al*. [49], although it may be responsible for some of the differences in $\delta^{18}O$ between symbiont-bearing species such as *Globigerinoides sacculifer*, *Globigerinoides ruber* and *Orbulina universa*. It does, however, seem to be more pronounced in data from certain genera of fossil planktonic foraminifera (see below). Figure 3 is a simple interpretative cartoon, modified from Pearson & Wade [66], summarizing these effects and how they can be identified in the fossil datasets used in this study.

5. Eocene reconstructions

We reconstructed water column $\delta^{13}C_{DIC}$ profiles for several Eocene time slices by the following four steps.

1. We plotted the $\delta^{18}O$ and $\delta^{13}C$ values for each species/size fraction against each other and used the criteria of Birch *et al*. [49,78] discussed above to identify those data points that are

considered to represent disequilibrium/upwelling effects or that plot along a mixing line between two distinct depth habitats (figure 3). We used an optimal growth stage/shell size window of 212–355 μm.

2. The $\delta^{18}O$ values for the chosen species/size fractions were converted into calcification temperatures, using the equation of Kim & O'Neil [79]. We used an Eocene ice volume correction of −0.75‰ according to Cramer *et al*. [80], and we applied a seawater latitude correction of +0.83 [81] assuming a palaeolatitude of 19° S.
3. The depth of calcification for each of these samples was estimated by fitting these $\delta^{18}O$ temperatures to modelled Eocene water column temperature profiles for offshore Tanzania and the southeast Gulf of Mexico [82,83].
4. We plotted the corresponding $\delta^{13}C$ values against the reconstructed calcification depth for each data point. The resulting Tanzanian $\delta^{13}C_{DIC}$–depth profiles were compared with the modern profile for offshore Tanzania (a composite of the profiles used in Birch *et al*. [49], from the World Ocean Database [60], is shown later in this section).

To carry out step 3, Eocene temperature–depth profiles for offshore Tanzania and the southeast part of the Gulf of Mexico were extracted from published Eocene general circulation model reconstructions. In the case of Tanzania, these were generated by the National Center for Atmospheric Research (NCAR) model and also the Hadley Centre Model version 3 (HadCM3) for comparison. The NCAR model profile [83] was generated for a continental margin adjacent to the East African coast centred around a latitude of approximately 18.2° S and for a slope extending from the water surface down to a water depth of 1500 m (figure 4). Experiments using different climate forcings of 1120, 2240 and 4480 ppmv atmospheric pCO_2 changed the absolute temperatures but not the shape of the temperature–depth profiles. We selected the profile generated by the pCO_2 condition that produced sea surface temperatures consistent with those estimated from the mixed-layer foraminiferal $\delta^{18}O$ data from our multi-species dataset [17]. For example, the profile generated using 4480 ppmv pCO_2 was used for the Early Eocene assemblages, and those generated using 2240 and 1120 ppmv pCO_2 were used for the Middle Eocene and Late Eocene time slices, respectively. In the different pCO_2 scenarios, the temperature gradient between the surface and 1500 m depth was always 18–20°C and, at all depths, even near the coast and at maximum water depths, most of the temperature gradient is above 600 m, i.e. this reconstruction should be relevant even for the shallower palaeodepth estimates. For the HadCM3 model [82], a forcing of 1680 ppmv pCO_2 was applied, and the generated profile (figure 4) represents that for a grid box centred around 41.25° E and 20° S for a water depth of up to approximately 4500 m. The shapes of the profiles generated by the two different models are consistent, and both show distinct differences compared with the modern profile for offshore Tanzania (from *in situ* temperature measurements; figure 4). Not only are the Eocene temperature–depth profiles offset to warmer temperatures over the entire water column compared with the modern Tanzania profile, but also the overall surface-to-deep temperature offsets are smaller. The thermocline is also broader in the Eocene profiles, with a roughly constant rate of temperature change down to 600 m compared with a modern thermocline that extends down to approximately 150 m. To determine the absolute depths for our foraminifera sample data, we used a logarithmic regression of the data generated by the NCAR model for a water depth of 600 m (as this was most consistent with the hemipelagic slope setting and benthic $\delta^{18}O$ temperature estimates). The $\delta^{18}O$-derived temperatures for each data point (derived in step 2) were input into the equation generated by this regression to give an absolute water depth. For the single dataset from the Guayabal Formation, Mexico, a temperature–depth profile was also generated using the NCAR model [83] and a climate forcing of 2240 ppmv pCO_2 for an area in the southeast part of the Gulf of Mexico from the coast down to 1500 m water depth (figure 4). Modern temperature–depth measurements for this area were obtained from the World Ocean Atlas database [84]; the curve in figure 4 represents a composite of seven profiles between 19.5 and 22.5° N and −95.5 and −96.5° W. Both profiles are also shown in figure 4.

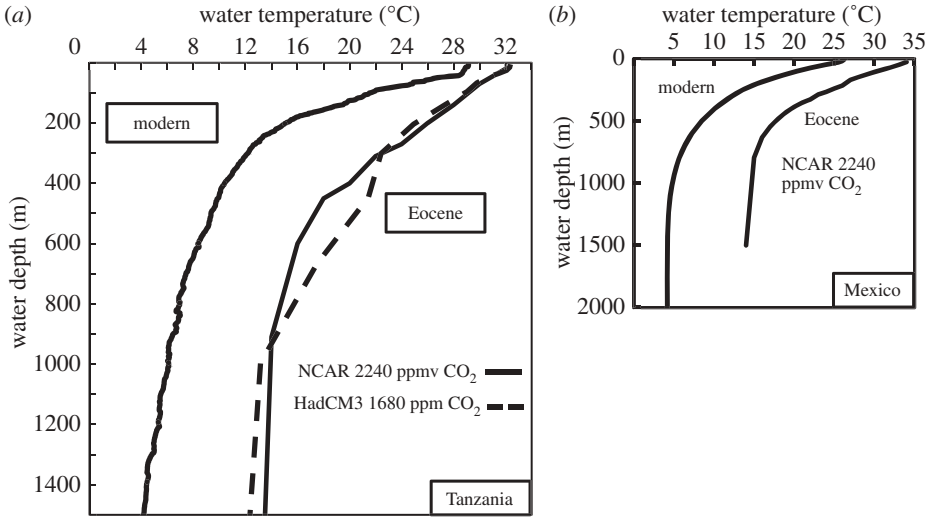

Figure 4. (*a*) Temperature–depth profiles from modern measurements from offshore Tanzania (CTD data from 41° 77 E, 10° 65 S, water depth 2219 m [58]) and those generated by HadCM3 (dashed line) and NCAR (solid line) models [82,83]. Only the NCAR profile produced using a 2240 ppmv pCO_2 climate forcing is illustrated here. The sea surface temperatures in the modelled profile are consistent with the temperatures derived from Middle Eocene mixed-layer foraminiferal $\delta^{18}O$ values. The profiles generated by 1120 ppmv (used for the Late Eocene time slice) and 4480 ppmv (used for the Early Eocene time slices) pCO_2 simply shift the profile to higher or lower temperatures. (*b*) Temperature–depth profile for the modern (a composite of seven measured depth profiles from the World Ocean Database [60] between 19.5 and 22.5° N and −95.5 and −96.5° W) and profile generated by the NCAR model for the Middle Eocene [83].

A logarithmic regression of the data generated by the NCAR model from the surface to a depth of approximately 300 m (consistent with the neritic zone palaeoenvironment of the Guayabal Formation) and absolute water depths determined as for Tanzania. The significance of the model results is discussed elsewhere [82,83].

The carbon and oxygen isotope cross-plots and the step-by-step reconstruction of the $\delta^{18}C_{DIC}$–depth profiles are illustrated in figure 5. The mixed-layer species, that is those with the lowest $\delta^{18}O$ values, in the Early and Middle Eocene samples are mainly from the muricate genera *Acarinina*, *Morozovella*, *Morozovelloides* and *Igorina*, which are interpreted as having had obligate symbiotic algae [70,87,88]. The majority of symbiotic $\delta^{18}C$ enrichment in these species, which has the effect of exaggerating the surface-to-deep $\delta^{13}C_{DIC}$ gradient, has been minimized by using only species within the 212–355 µm test size range, as discussed above (figure 5*a–f*(ii)). Other near-surface calcifiers include the apparently non-symbiotic genera *Pseudohastigerina, Planoglobanomalina* [89] and *Chiloguembelina* [90]. Other genera present include *Dentoglobigerina, Turborotalia, Parasubbotina, Subbotina, Hantkenina* and *Catapsydrax*, whose lower $\delta^{13}C$ and higher $\delta^{18}O$ values indicate calcification at greater depths. Species belonging to the genera *Globigerinatheka*, *Orbulinoides* and *Guembelitrioides* tend to have isotopic compositions suggestive of mixed-layer calcification followed by further gametogenic calcification at greater depth. This is consistent with observations, as these genera typically show gametogenic calcite crusts [87,91]; hence, these data were not used to generate the $\delta^{13}C$–depth profiles (figure 5).

The one Late Eocene assemblage (figure 5*g*) differs in composition from the others, in part due to the large assemblage turnover in planktonic foraminifera in the Late Middle Eocene that resulted in the extinction of the morozovelloidids and larger acarininids [92]. Constructing a realistic $\delta^{13}C$ profile for this assemblage is problematic given the limited mixed-layer data. We include the plots for completeness but restrict our interpretation to the Early and Middle Eocene reconstructions pending further investigation of Late Eocene assemblages.

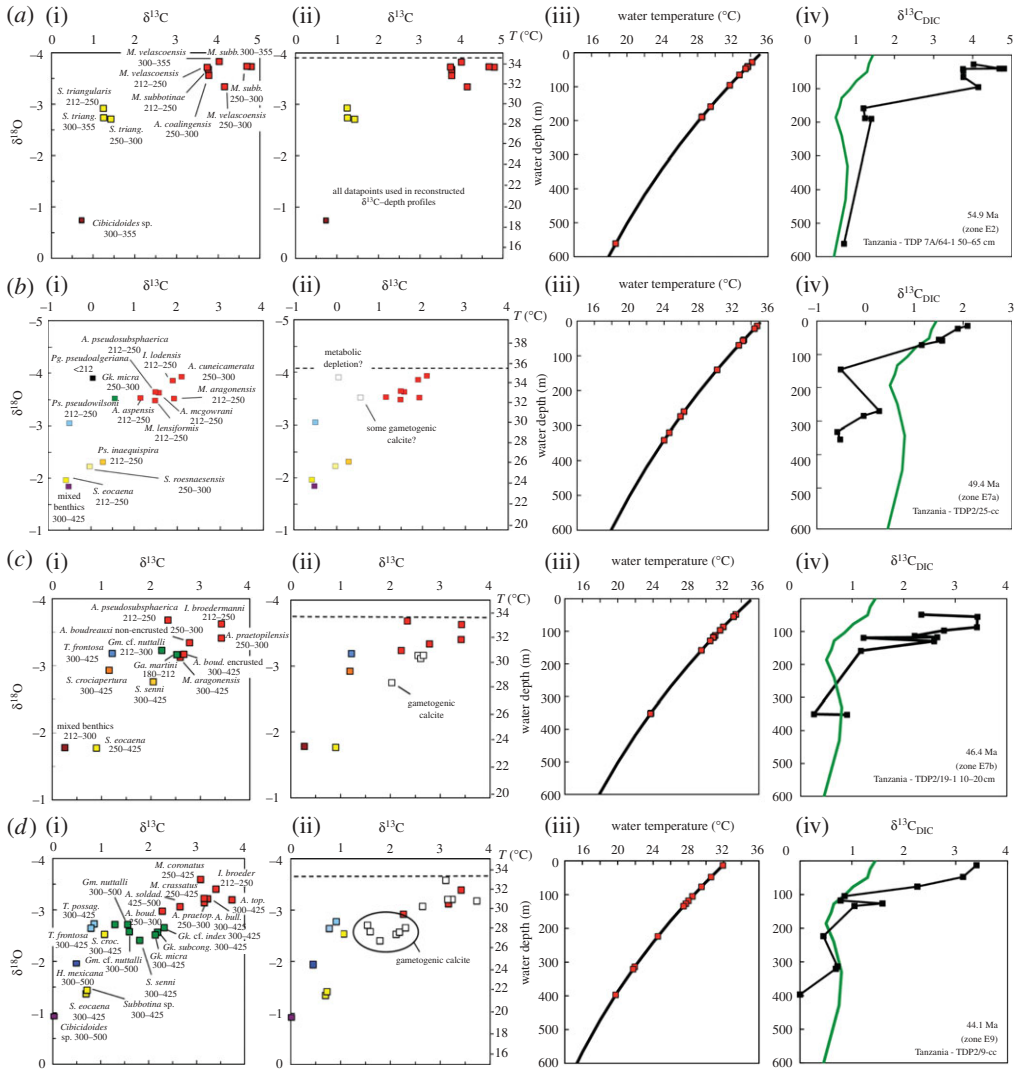

Figure 5. (*a–h*) Step-by-step reconstruction of $\delta^{13}C$–depth gradients using these data and modelled temperature–depth profiles. (i) Cross-plots of $\delta^{13}C$ and $\delta^{18}O$ data from Pearson *et al*. [17,51] and Wade & Pearson [50] showing names of multiple species of planktonic (and benthic) foraminifera and the size fraction in which they were analysed (given in μm), where appropriate. Note that in (*h*) species names have been updated from the original dataset in Pearson *et al*. [51]. **Ps. pseudowilsoni* in this case was originally named *Paragloborotalia pseudomayeri* in Pearson *et al*. [51]. Strictly speaking, *Pa. pseudomayeri* is a synonym of *Turborotalia pomeroli* [85] but at the time of data collection, the authors [51] actually designated this species name to what would now be referred to as *Ps. pseudowilsoni*. *A., Acarinina*; *C., Catapsydrax*; *Cb., Cribrohantkenina*; *Cg., Chiloguembelina*; *Ga., Globoturborotalita*; *Gk., Globigerinatheka*; *Gm., Guembelitrioides*; *I., Igorina*; *M., Morozovella* in (*a–c*), *Morozovelloides* in (*d–f*); *Pg., Planoglobanomalina*; *Ph., Pseudohastigerina*; *Ps., Parasubbotina*; *S., Subbotina*; *Ta., Turborotalita*. (ii) The same cross-plots redrawn to show mixed-layer temperature (generated from the lowest $\delta^{18}O$ value), denoted by a dashed line. Empty squares represent those data points that were not used to construct the final $\delta^{13}C$ profile following the criteria of Birch *et al*. [78]. Note that no data points were eliminated from the Guayabal Formation assemblage (*h*) because, during the initial data collection, foraminifera were chosen from all size fractions more than 250 μm. (iii) Temperature–depth profile showing how the $\delta^{18}O$-generated temperatures were used to generate absolute depths. (iv) $\delta^{13}C$–depth profiles for each sample (black) and the modern profile (green) for offshore Tanzania (averaged profile from several nearby sites). Note that studies suggest that surface Indian Ocean $\delta^{13}C_{DIC}$ values have decreased by approximately 0.6‰ since 1900 [86] owing to the 'Suess effect', i.e. the influence of isotopically light carbon emitted through burning fossil fuels. This has not been included in the figure but should be noted.

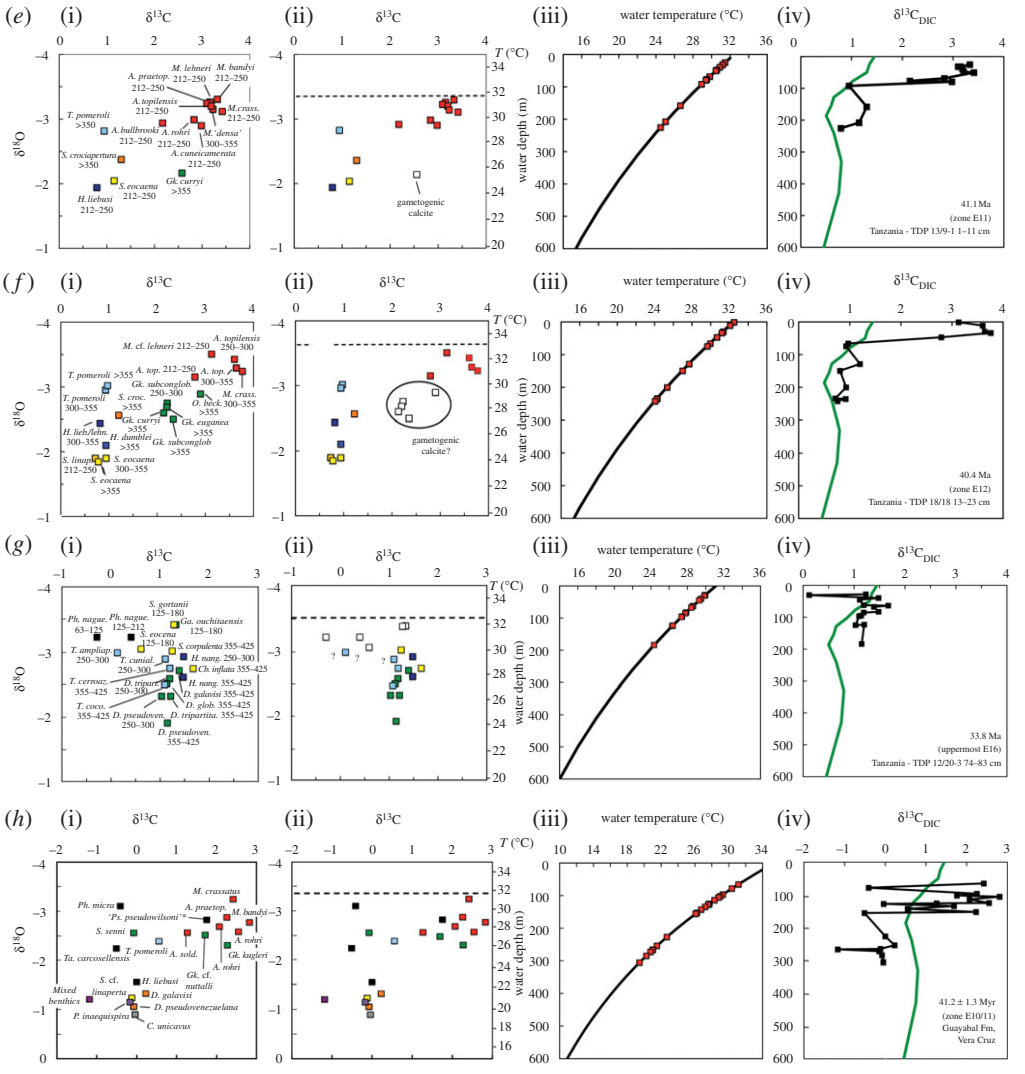

Figure 5. (*Continued*).

There are two common features to the Early and Middle Eocene profiles.

1. The carbon isotope profile appears to have been much steeper through the upper thermocline than is typical of the oceans in this area and most of the world. The modern $\delta^{13}C$ profile for this part of the Indian Ocean [49,60] shows a fairly constant rate of decrease down to approximately 1 km, with little change beyond this depth. Conversely, the Early and Middle Eocene profiles consistently show a sharp decrease in $\delta^{13}C$ concentrated between the mixed layer and approximately 100–150 m depth.
2. The overall surface-to-deep offsets in the Early and Middle Eocene $\delta^{13}C$ profiles are large relative to today, even when the Suess effect is taken into account. In the modern western Indian Ocean, at this latitude, the total gradient is approximately 1–1.5‰. On a global scale, modern surface-to-deep gradients rarely exceed 2‰ [23]. Similar gradients have also characterized at least the past 20 million years [93]. However, the Early and Middle Eocene profiles show $\delta^{13}C$ offsets of 2–4‰. Similar values and overall surface-to-deep gradients (2–3‰) have been previously reported for the Early and Middle Eocene even from recrystallized foraminifera from a variety of latitudes in the Atlantic, Pacific, Indian and Mediterranean basins [51,54,94]. Recrystallization should dampen surface-to-deep

$\delta^{13}C$ gradients as measured in foraminifera tests, and so many of these datasets may underestimate the offsets. In terms of absolute values, surface values in our dataset are mostly elevated compared with today; deepwater values are comparable.

We consider it unlikely that features 1 and 2 are an artefact of the modelled water column temperature–depth profile. For example, if the modelled profiles had underestimated the temperature gradient in the upper ocean and the profile shape was more similar to the modern, then the reconstructed $\delta^{13}C_{DIC}$–depth gradients would be even steeper through the upper thermocline, as the range of $\delta^{18}O$ values (and therefore temperature) measured in the assemblage is small. However, if the models had *overestimated* the temperature–depth gradient, and water column temperatures were actually more vertically homogeneous, we could admittedly have generated a $\delta^{13}C_{DIC}$–depth gradient that was artificially steep in the upper ocean. Nonetheless, the large range of $\delta^{13}C_{DIC}$ values measured in the Tanzanian and Mexican foraminifera assemblages suggests that strong vertical mixing was not occurring at those sites.

Another potential source of uncertainty relates to the issue of Eocene water depths and coastal proximity, which can be difficult to determine precisely for hemipelagic deposits and may have varied with time. The Kilwa Group of Tanzania comprises several kilometre successions of relatively monotonous clays and claystones with occasional turbidite interbeds [55,56]. The palaeoshoreline is estimated to have been generally approximately 50 km from the site of deposition [95] and palaeodepths have previously been estimated at 300–500 m based on upper bathyal benthic foraminiferal assemblages [56]. However, the deeper limit of this estimate is uncertain, and given the narrow shelf and steep slope that is typical of the East Africa margin, it is quite possible that palaeodepths were considerably greater than this. Both the foraminifera and nanofossil assemblages indicate a fairly constant, open, deep and relatively oligotrophic environment; there are no restricted assemblages or conspicuous shelf-restricted or eutrophic taxa [52]. Coring of modern hemipelagic sediments offshore of Tanzania has revealed that silty clays of similar facies to the Kilwa Group are currently being deposited at depths of 500–1800 m within 50 km of the shoreline [58]; hence, a more conservative depth estimate for the Eocene sediments would be 300–1800 m. For both modern and Eocene environments, it is likely that onshore currents brought gyre water onto the continental slope, lending an oceanic rather than coastal character to the water column. Therefore, although we acknowledge that these issues do introduce uncertainty into our approach, we argue that we cannot rule out the idea that the Eocene and modern datasets represent similar palaeoenvironments.

In addition, although all Eocene planktonic foraminifera are extinct, we can envisage no plausible vital effect or other fractionation factor that would have affected the surface-dwelling forms in a way that could produce such heavy $\delta^{13}C$ values as seen in figure 5. Even if we have inadvertently included values affected by symbiotic effects, such effects are only approximately 1‰ or less in the modern and can therefore not explain the differences fully. An obvious question, then, is to ask whether these surface dwellers had more pronounced symbiotic effects than modern forms. It may also be that the isotopic fractionation factor associated with primary production (i.e. that associated with symbionts) was higher before the Late Eocene owing to effects relating to elevated pCO_2 levels, growth rates and/or volume-to-surface-area ratios in primary producers [96,97]. However, published relationships between $\delta^{13}C$ and test size for muricate species (acarininids and morozovellids) from warm Palaeocene/Eocene oceans have gradients similar to or indeed shallower than modern planktonic foraminifera with obligate symbionts, such as *Gs. ruber* and *Gs. sacculifer* [70,78,98,99], suggesting that, if anything, the symbiotic effect was less pronounced. Hence, the data suggest that vertical carbon cycling operated very differently in the Early and Middle Eocene than is typical in the modern ocean.

6. Interpretation

The fact that the $\delta^{13}C_{DIC}$ decreases so sharply through the upper thermocline and to such a degree in the Eocene time slices compared with most modern oceanic environments is notable.

One control on the depth of the $\delta^{13}C_{DIC}$ minimum is oceanic circulation, and different oceanic circulation/mixing patterns in the Eocene compared with the modern, for example a shallower mixed layer (perhaps due to reduced wind-induced mixing) or enhanced oceanic stratification relating to a warmer climate, could have contributed to the sharper, shallower decrease in $\delta^{13}C_{DIC}$. Additionally, faster rates of remineralization of sinking organic matter below the mixed layer could partly explain the shape of the profile. Indeed, the shape of the profiles implies that the majority of remineralization of sinking organic matter was occurring at a much shallower depth than is typical in the modern. Reconstructed sea surface temperatures offshore of Tanzania and in the Gulf of Mexico in the Eocene were only 2–4°C greater than today, which is not sufficient to affect remineralization rates greatly, particularly at temperatures so much higher than 20°C. However, at a depth of around 150 m, Eocene water temperatures were approximately 10°C higher than today (figure 4) [82,83]. This means that if, for example, heterotrophic community respiration had a Q_{10} value of 2 (a conservative estimate [6]), then respiration rates could quite reasonably have been twice as high at these depths as in the modern. Therefore, any temperature-related increase in microbial metabolic activity rates would have been more pronounced below the mixed layer than at the surface, that is, in the zone of net respiration rather than net photosynthesis. We acknowledge that there are controls on the shape of the vertical $\delta^{13}C_{DIC}$ profile other than temperature-dependent remineralization and that to understand how these factors affect how $\delta^{13}C_{DIC}$ changes with depth requires detailed modelling. However, we propose here that the shape of the $\delta^{18}C_{DIC}$–depth profile could have resulted, at least in part, from the fact that there was a much greater temperature difference at depths below the mixed layer (figure 4), which, in turn, led to more rapid rates of organic matter remineralization.

If biogenic remineralization of organic carbon was more efficient in the Eocene water column owing to elevated water temperatures, given that warmer-than-modern water temperatures extended to high latitudes, then these findings may have had global significance. As proposed by Olivarez Lyle & Lyle [24], Stanley [25] and other authors focusing on the importance in terms of modern climates [3,4,6], this may have affected the transport of organic matter to the deep ocean and may have ultimately reduced rates of organic carbon burial and indeed inorganic burial through an increase in the DIC reservoir and shoaling of the CCD. This could have pushed pCO_2 levels even higher, thus supporting a positive feedback mechanism keeping pCO_2 levels high during greenhouse periods (when remineralization rates are high) and low during icehouse conditions (when remineralization rates are lower). However, the possibility of global effects is probably best investigated using carbon cycle modelling, because, for example, any consideration of impacts on the global carbon cycle must take into account parameters such as organic carbon burial and remineralization rates in continental shelf environments [97,100,101]. Rapid subsurface bacterial remineralization would have caused a marked upward displacement of the oxygen minimum zone, which would, in turn, have affected the locus and rate of organic carbon deposition on the continental shelves and margins [25]. Moreover, on long time scales (e.g. 10^3–10^6 years), negative feedback mechanisms caused by enhanced silicate weathering could counteract any increases in pCO_2 caused by a reduction in deep-sea carbon burial [100,102,103].

The second observation, that is, the larger surface-to-deep $\delta^{13}C$ gradient, has been reported in several cases and seems to be a common feature of the Eocene ocean [54,94]. More complete remineralization of organic matter should in theory produce a greater surface-to-deep offset, as more light carbon is being pumped into the ocean interior, although this is unlikely to be the sole cause of the elevated gradients. More complete remineralization should serve to reduce the $\delta^{13}C_{DIC}$ in the deeper ocean rather than elevate surface values. Instead, the surface ocean $\delta^{13}C_{DIC}$ could have been elevated due to higher rates of primary productivity, which would have transferred proportionally more ^{12}C to organic tissues than occurs today. This would imply higher oceanic nutrient availability, perhaps from enhanced silicate weathering under greenhouse climates [100,101,103,104] or efficient turnover of deepwaters [105]. Alternatively, oceanic DIC concentrations could have been generally lower in the Eocene, as indicated by some carbon cycle

models [101], which would enhance observed $\delta^{13}C_{DIC}$–depth gradients even without a change in rates of primary productivity in the surface ocean. This remains a possibility, although several models suggest broadly unchanged DIC (and alkalinity) over the Cenozoic [106].

In summary, our data from the warm Eocene ocean provide *prima facie* support for the idea that the remineralization of sinking organic carbon in the water column was much more efficient than is currently the case, and that the majority of remineralization occurred much higher in the water column. We plan to investigate this possibility further by incorporating metabolic rate effects into carbon cycle models. Models should also be used to take into account other controls on the shape of the $\delta^{13}C_{DIC}$–depth profile, many of which may relate to elevated water temperatures, such as changes in oceanic circulation and enhanced oceanic stratification. This information about warm climates from the past may have important implications for the future: if anthropogenic emissions move the world oceans towards warm Eocene-like conditions, there may be similar profound consequences for water column structure and biological activity, and potentially far-reaching effects on the marine carbon cycle.

Acknowledgements. We thank M. Huber and J. Tindall for their contribution to the Eocene modelled temperature–depth profiles.

Funding statement. This work was supported by a NERC standard grant awarded to G.L.F. and P.N.P.

References

1. Kleypas JA, Buddemeier RW, Archer D, Gattuso J-P, Langdon C, Opdyke BN. 1999 Geochemical consequences of increased atmospheric carbon dioxide on coral reefs. *Science* **284**, 117–120. (doi:10.1126/science.284.5411.118)
2. Caldeira K, Wicket ME. 2003 Anthropogenic carbon and ocean pH. *Nature* **425**, 365. (doi:10.1038/425365a)
3. Laws EA, Falkowski PG, Smith WO, Ducklow H, McCarthy JJ. 2000 Temperature effect on export production in the open ocean. *Glob. Biogeochem. Cycles* **14**, 1231–1246. (doi:10.1029/1999GB001229)
4. Matsumoto K. 2007 Biology-mediated temperature control on atmospheric pCO_2 and ocean biogeochemistry. *Geophys. Res. Lett.* **34**, L20605. (doi:10.1029/2007GL031301)
5. Young KE, Primeau F, Sarmiento JL. 2009 The impact of remineralisation depth on the air–sea carbon balance. *Nat. Geosci.* **2**, 630–635. (doi:10.1038/ngeo612)
6. Regaudie-de-Gioux A, Duarte CM. 2012 Temperature dependence of planktonic metabolism in the ocean. *Glob. Biogeochem. Cycles* **26**, GB1015. (doi:10.1029/2010GB003907)
7. Sloan LC, Rea DK. 1995 Atmospheric carbon dioxide and early Eocene climate: a general circulation modeling sensitivity study. *Palaeogeogr. Palaeoclimatol. Palaeoecol.* **119**, 275–295. (doi:10.1016/0031-0182(95)00012-7)
8. Markwick PJ. 1998 Fossil crocodilians as indicators of late Cretaceous and Cenozoic climates: implications for using palaeontological data in reconstructing palaeoclimate. *Palaeogeogr. Palaeoclimatol. Palaeoecol.* **137**, 205–271. (doi:10.1016/S0031-0182(97)00108-9)
9. Huber M. 2009 Climate change: snakes tell a torrid tale. *Nature* **457**, 669–671. (doi:10.1038/457669a)
10. Greenwood DR. 2007 Fossil angiosperm leaves and climate: from Wolfe and Dilcher to Burnham and Wilf. *Advances in Angiosperm Paleobotany and Paleoclimatic Reconstruction—Contributions Honouring David L. Dilcher and Jack A. Wolfe* (eds DM Jarzen, SR Manchester, GJ Retallack, SA Jarzen). Courier Forschungsinstitut Senckenberg, vol. 258, pp. 95–108. Stuttgart, Germany: Schweizerbart.
11. Shackleton NJ, Kennett JP. 1975 Paleotemperature history of the Cenozoic and the initiation of Antarctic glaciation: oxygen and carbon isotope analyses in DSDP sites 277, 279, and 281. *Initial Rep. Deep Sea Drilling Project* **29**, 743–755.
12. Pearson P. 2012 Oxygen isotopes in foraminifera: overview and historical review. In *Reconstructing Earth's deep-time climate: the state of the art in 2012* (eds LC Ivany, BT Huber), pp. 1–38. Paleontological Society Papers 18. New Haven, CT: Yale University Press.
13. Zachos J, Pagani M, Sloan L, Thomas E, Billups K. 2001 Trends, rhythms, and aberrations in global climate 65 Ma to present. *Science* **292**, 686–693. (doi:10.1126/science.1059412)

14. Zachos JC, Dickens GR, Zeebe RE. 2008 An Early Cenozoic perspective on greenhouse warming and carbon-cycle dynamics. *Nature* **451**, 279–283. (doi:10.1038/nature06588)
15. Bohaty SM, Zachos JC. 2003 Significant Southern Ocean warming event in the late middle Eocene. *Geology* **31**, 1017–1020. (doi:10.1130/G19800.1)
16. Edgar K, Wilson P, Sexton P, Gibbs S, Roberts A, Norris R. 2010 New biostratigraphic, magnetostratigraphic and isotopic insights into the Middle Eocene Climatic Optimum in low latitudes. *Palaeogeogr. Palaeoclimatol. Palaeoecol.* **297**, 670–682. (doi:10.1016/j.palaeo.2010.09.016)
17. Pearson PN, van Dongen BE, Nicholas CJ, Pancost RD, Schouten S, Singano JM, Wade BS. 2007 Stable warm tropical climate through the Eocene epoch. *Geology* **35**, 211–214. (doi:10.1130/G23175A.1)
18. Bijl PK, Schouten S, Sluijs A, Reichart G-J, Zachos JC, Brinkhuis H. 2009 Early Palaeogene temperature evolution of the southwest Pacific Ocean. *Nature* **461**, 776–779. (doi:10.1038/nature08399)
19. Liu Z, Pagani M, Zinniker D, DeConto RM, Huber M, Brinkhuis H, Shah SR, Leckie RM, Pearson A. 2009 Global cooling during the Eocene–Oligocene climate transition. *Science* **323**, 1187–1190. (doi:10.1126/science.1166368)
20. Emanuel K, Des Autels C, Holloway C, Korty R. 2004 Environmental control of tropical cyclone intensity. *J. Atmos. Sci.* **61**, 843–858. (doi:10.1175/1520-0469(2004)061<0843:ECOTCI>2.0.CO;2)
21. Sriver RL, Huber M. 2007 Observational evidence for an ocean heat pump induced by tropical cyclones. *Nature* **447**, 557–580. (doi:10.1038/nature05785)
22. Sigman DM, Haug GH. 2003 The biological pump in the past. In *Treatise on geochemistry* (eds HD Holland, KK Turekian, H Elderfield), pp. 491–528. Oxford, UK: Elsevier Science.
23. Kroopnick PM. 1985 The distribution of ^{13}C of $\sum CO_2$ in the world oceans. *Deep Sea Res.* **32**, 57–84. (doi:10.1016/0198-0149(85)90017-2)
24. Olivarez Lyle A, Lyle MW. 2006 Missing organic carbon in Eocene marine sediments: Is metabolism the biological feedback that maintains end-member climates? *Paleoceanography* **21**, PA2007. (doi:10.1029/2005PA001230)
25. Stanley SM. 2010 Relation of Phanerozoic stable isotope excursions to climate, bacterial metabolism, and major extinctions. *Proc. Natl Acad. Sci. USA* **107**, 19 185–19 189. (doi:10.1073/pnas.1012833107)
26. Spero HJ, Lerche I, Williams DF. 1991 Opening the carbon isotope 'vital effect' black box, 2. Quantitative model for interpreting foraminiferal carbon isotope data. *Paleoceanography* **6**, 639–655. (doi:10.1029/91PA02022)
27. Arrhenius S. 1889 Uber die Reaktionsgeschwindigkeit bei der Inversion von Rohrzucker durch Säuren. *Z. Phys. Chem.* **4**, 226–248.
28. Hargrave BT. 1969 Similarity of oxygen uptake by benthic communities. *Limnol. Oceanogr.* **14**, 801–805. (doi:10.4319/lo.1969.14.5.0801)
29. Singh JS, Gupta SR. 1977 Plant decomposition and soil respiration in terrestrial ecosystems. *Bot. Rev.* **43**, 449–528. (doi:10.1007/BF02860844)
30. Swart PK. 1983 Carbon and oxygen isotope fractionation in scleractinian corals: a review. *Earth Sci. Rev.* **19**, 51–80. (doi:10.1016/0012-8252(83)90076-4)
31. Hobbie JE, Cole JJ. 1984 Response of a detrital food web to eutrophication. *Bull. Mar. Sci.* **35**, 357–363.
32. White PA, Kalff J, Rasmussen JB, Gasol JM. 1991 The effect of temperature and algal biomass on bacterial production and specific growth rate in freshwater and marine habitats. *Microbial Ecol.* **21**, 99–118. (doi:10.1007/BF02539147)
33. Brown JH, Gillooly JF, Allen AP, Savage VM, West GB. 2004 Toward a metabolic theory of ecology. *Ecology* **85**, 1771–1789. (doi:10.1890/03-9000)
34. Gillooly JF, Brown JH, West GB, Savage VM, Charnov EL. 2001 Effects of size and temperature on metabolic rate. *Science* **293**, 2248–2251. (doi:10.1126/science.1061967)
35. Gillooly JF, Charnov EL, West GB, Savage VM, Brown JH. 2002 Effects of size and temperature on developmental time. *Nature* **417**, 70–73. (doi:10.1038/417070a)
36. Harris LA, Duarte CM, Nixon SW. 2006 Allometric laws and prediction in estuarine and coastal ecology. *Estuaries Coasts* **29**, 340–344. (doi:10.1007/BF02782002)
37. López-Urrutia A, San Martin E, Harris RP, Irigoyen X. 2006 Scaling the metabolic balance of the oceans. *Proc. Natl Acad. Sci. USA* **103**, 8739–8744. (doi:10.1073/pnas.0601137103)

38. Hoppe HG, Gocke K, Koppe R, Begler C. 2002 Bacterial growth and primary production along a north–south transect of the Atlantic Ocean. *Nature* **416**, 168–171. (doi:10.1038/416168a)
39. Chikamoto MO, Abe-Ouchi A, Oka A, Smith SL. 2012 Temperature induced marine export production during glacial period. *Geophys. Res. Lett.* **39**, L21601. (doi:10.1029/2012GL053828)
40. Gu G, Dickens GR, Bhatnagar G, Colwell FS, Hirasaki GJ, Chapman WG. 2011 Abundant early Palaeogene marine gas hydrates despite warm deep-ocean temperatures. *Nat. Geosci.* **4**, 848–851. (doi:10.1038/ngeo1301)
41. Berner RA, Caldeira K. 1997 The need for mass balance and feedback in the geochemical carbon cycle. *Geology* **25**, 955–956. (doi:10.1130/0091-7613(1997)025<0955:TNFMBA>2.3.CO;2)
42. Armstrong RA, Lee C, Hedges JL, Honjo S, Wakeham SG. 2002 A new, mechanistic model for organic carbon fluxes in the ocean, based on the quantitative association of POC with ballast minerals. *Deep Sea Res. II* **49**, 219–236. (doi:10.1016/S0967-0645(01)00101-1)
43. François R, Honjo S, Krishfield R, Manganini S. 2002 Factors controlling the flux of organic carbon to the bathypelagic zone of the ocean. *Glob. Biogeochem. Cycles* **16**, 34. (doi:10.1029/2001GB001722)
44. Klaas C, Archer D. 2002 Association of sinking organic matter with various types of mineral ballast in the deep sea: implications for the rain ratio. *Glob. Biogeochem. Cycles* **16**, 63. (doi:10.1029/2001GB001765)
45. Wilson JD, Barker S, Ridgwell A. 2012 Assessment of the spatial variability in particulate organic matter and mineral sinking fluxes in the ocean interior: implications for the ballast hypothesis. *Glob. Biogeochem. Cycles* **26**, GB4011. (doi:10.1029/2012GB004398)
46. Hemleben CH, Spindler M, Anderson OR. 1989 *Modern planktonic foraminifera*. Berlin, Germany: Springer.
47. Emiliani C. 1954 Depth habitats of some species of pelagic foraminifera as indicated by oxygen isotope ratios. *Am. J. Sci.* **252**, 149–158. (doi:10.2475/ajs.252.3.149)
48. Zeebe RE, Bijma J, Wolf-Gladrow DA. 1999 A diffusion–reaction model of carbon isotope fractionation in foraminifera. *Mar. Chem.* **64**, 199–227. (doi:10.1016/S0304-4203(98)00075-9)
49. Birch H, Coxall HK, Pearson PN, Kroon D, O'Regan M. 2013 Planktonic foraminifera stable isotopes and water column structure: disentangling ecological signals. *Mar. Micropaleontol.* **101**, 127–145. (doi:10.1016/j.marmicro.2013.02.002)
50. Wade BS, Pearson PN. 2008 Planktonic foraminiferal turnover, diversity fluctuations and geochemical signals across the Eocene/Oligocene boundary in Tanzania. *Mar. Micropaleontol.* **68**, 244–255. (doi:10.1016/j.marmicro.2008.04.002)
51. Pearson PN, Ditchfield P, Singano J, Harcourt-Brown K, Nicholas C, Olsson R, Shackleton NJ, Hall M. 2001 Warm tropical sea surface temperatures in the late Cretaceous and Eocene epochs. *Nature* **413**, 481–487. (doi:10.1038/35097000)
52. Bown PR *et al*. 2008 A Paleogene calcareous microfossil Konservat-Lagerstätte from the Kilwa Group of coastal Tanzania. *Geol. Soc. Am. Bull.* **120**, 3–12. (doi:10.1130/B26261.1)
53. Sexton PF, Wilson PA, Pearson PN. 2006 Palaeoecology of late middle Eocene planktic foraminifera and evolutionary implications. *Mar. Micropaleontol.* **60**, 1–16. (doi:10.1016/j.marmicro.2006.02.006)
54. Hilting AK, Kump LR, Bralower TJ. 2008 Variations in the oceanic vertical carbon isotope gradient and their implications for the Paleocene–Eocene biological pump. *Paleoceanography* **23**, PA3222. (doi:10.1029/2007PA001458)
55. Pearson PN *et al.* 2004 Paleogene and Cretaceous sediment cores from the Kilwa and Lindi areas of coastal Tanzania: Tanzania Drilling Project Sites 1–5. *J. Afr. Earth Sci.* **39**, 25–62. (doi:10.1016/j.jafrearsci.2004.05.001)
56. Nicholas CJ *et al*. 2006 Stratigraphy and sedimentology of the Upper Cretaceous to Paleogene Kilwa Group, southern coastal Tanzania. *J. Afr. Earth Sci.* **45**, 431–466. (doi:10.1016/j.jafrearsci.2006.04.003)
57. Wade BS, Pearson PN, Berggren WA, Pälike H. 2011 Review and revision of Cenozoic tropical planktonic foraminiferal biostratigraphy and calibration to the Geomagnetic Polarity and Astronomical Time Scale. *Earth Sci. Rev.* **104**, 111–142. (doi:10.1016/j.earscirev.2010.09.003)
58. Kroon D, the Shipboard Scientific Party. 2010 GLOW: tropical temperature history during Paleogene global warming (GLOW) events. Site Survey Cruise Report, 151 pp.
59. Erez J, Luz B. 1983 Experimental paleotemperature equation for planktonic foraminifera. *Geochim. Cosmochim. Acta* **47**, 1025–1031. (doi:10.1016/0016-7037(83)90232-6)

60. National Oceanographic Data Center. World Ocean Database. 2009 See http://www.nodc.noaa.gov/OC5/WOD09/pr_wod09.html.
61. Berger WH, Killingley JS, Vincent E. 1978 Stable isotopes in deep-sea carbonates: box core ERDC-92, west equatorial Pacific. *Oceanol. Acta* **1**, 203–216.
62. Wefer G, Berger WH. 1991 Isotope paleontology: growth and composition of extant calcareous species. *Mar. Geol.* **100**, 207–248. (doi:10.1016/0025-3227(91)90234-U)
63. Ortiz JD, Mix AC, Rugh W, Watkins JM, Collier RW. 1996 Deep-dwelling planktonic foraminifera of the northeastern Pacific Ocean reveal environmental control of oxygen and carbon isotopic disequilibria. *Geochim. Cosmochim. Acta* **60**, 4509–4523. (doi:10.1016/S0016-7037(96)00256-6)
64. Spero HJ, Bijma J, Lea DW, Bemis BE. 1997 Effect of seawater carbonate concentration on foraminiferal carbon and oxygen isotopes. *Nature* **390**, 497–500. (doi:10.1038/37333)
65. Schmidt DN, Elliott T, Kasemann SA. 2008 The influences of growth rates on planktic foraminifers as proxies for palaeostudies – a review. In *Biogeochemical controls on palaeoceanographic environmental proxies* (eds WEN Austin, RH James). Geological Society Special Publication, no. 303, pp. 73–85. London, UK: Geological Society of London.
66. Pearson PN, Wade BS. 2009 Taxonomy and stable isotope paleoecology of well-preserved planktonic foraminifera from the uppermost Oligocene of Trinidad. *J. Foraminiferal Res.* **39**, 191–217. (doi:10.2113/gsjfr.39.3.191)
67. Bé AWH. 1982 Biology of planktonic foraminifera. In *Foraminifera notes for a short course* (eds MA Buzas, BK Sen Gupta, TW Broadhead), pp. 51–89. Knoxville, TN: University of Tennessee.
68. Bouvier-Soumagnac Y, Duplessy JC. 1985 Carbon and oxygen isotopic composition of planktonic foraminifera from laboratory culture, plankton tows and recent sediment: implications for the reconstruction of paleoclimatic conditions and of the global carbon cycle. *J. Foraminiferal Res.* **15**, 302–320. (doi:10.2113/gsjfr.15.4.302)
69. Spero HJ, Williams DF. 1988 Extracting environmental information from planktonic foraminiferal δ^{13}C data. *Nature* **335**, 717–719. (doi:10.1038/335717a0)
70. D'Hondt S, Zachos JC, Schultz G. 1994 Stable isotopic signals and photosymbiosis in late Paleocene planktic foraminifera. *Palaeobiology* **20**, 391–406.
71. Norris RD. 1996 Symbiosis as an evolutionary innovation in the radiation of Paleocene planktic foraminifera. *paleobiology* **22**, 461–48.
72. Spero HJ, Lea DW. 1996 Experimental determination of stable isotope variability in *Globigerina bulloides*: implications for paleoceanographic reconstructions. *Mar. Micropaleontol.* **28**, 231–246. (doi:10.1016/0377-8398(96)00003-5)
73. Bijma J, Spero HJ, Lea DW. 1999 Reassessing foraminiferal stable isotope geochemistry: impact of the oceanic carbonate system (experimental results). In *Use of proxies in paleoceanography: examples from the South Atlantic* (eds G Fischer, G Wefer), pp. 489–521. New York, NY: Springer.
74. Duplessy JC, Delibrias G, Turon JL, Pujol C, Duprat J. 1981 Deglacial warming of the northeastern Atlantic Ocean: correlation with the paleoclimatic evolution of the European continent. *Palaeogeogr. Palaeoclimatol. Palaeoecol.* **35**, 121–144. (doi:10.1016/0031-0182(81)90096-1)
75. Kroon D, Darling K. 1995 Size and environmental control of the stable isotope signal related to test size in *Neogloboquadrina dutertrei* (d'Orbigny) and *Globigerinoides ruber* d'Orbigny. *J. Foraminiferal Res.* **25**, 39–52. (doi:10.2113/gsjfr.25.1.39)
76. Triantaphyllou MV, Antonarakou A, Dimiza M, Anagnostou CH. 2010 Calcareous nannofossil and planktonic foraminiferal distributional patterns during deposition of sapropels S6, S5 and S1 in the Libyan Sea (Eastern Mediterranean). *Geo-Marine Lett.* **30**, 1–13. (doi:10.1007/s00367-009-0145-7)
77. Chaisson WP, Ravelo AC. 1997 Changes in upper water-column structure at site 925, late Miocene–Pleistocene: planktonic foraminifer assemblage and isotopic evidence. In *Proc. Ocean Drilling Program, Scientific Results*, vol. 154 (eds NJ Shackleton, WB Curry, C. Richter, TJ Bralower), pp. 255–268. College Station, TX: Ocean Drilling Program. (doi:10.2973/odp.proc.sr.154.105.1997)
78. Birch HB, Coxall HK, Pearson PN. 2012 Evolutionary ecology of early Paleocene planktonic foraminifera: size, depth habitat and symbiosis. *Paleobiology* **38**, 374–390. (doi:10.1666/11027.1)

79. Kim S-T, O'Neil JR. 1997 Equilibrium and non-equilibrium oxygen isotope effects in synthetic carbonates. *Geochim. Cosmochim. Acta* **61**, 3461–3475. (doi:10.1016/S0016-7037(97)00169-5)
80. Cramer BS, Miller KG, Barrett PJ, Wright JD. 2011 Late Cretaceous–Neogene trends in deep ocean temperature and continental ice volume: reconciling records of benthic foraminiferal geochemistry (δ^{18}O and Mg/Ca) with sea level history. *J. Geophys. Res. Oceans* **116**, C12023. (doi:10.1029/2011JC007255)
81. Zachos JC, Stott LD, Lohmann KC. 1994 Evolution of early Cenozoic marine temperatures. *Paleoceanography* **9**, 353–387. (doi:10.1029/93PA03266)
82. Tindall JC, Flecker R, Valdes P, Schmidt DN, Markwick P, Harris J. 2010 Modelling the oxygen isotope distribution of ancient seawater using a coupled ocean–atmosphere GCM: implications for reconstructing early Eocene climate. *Earth Planet. Sci. Lett.* **292**, 265–273. (doi:10.1016/j.epsl.2009.12.049)
83. Huber M, Caballero R. 2011 The early Eocene equable climate problem revisited. *Clim. Past Discuss.* **7**, 241–304. (doi:10.5194/cpd-7-241-2011)
84. National Oceanographic Data Center. World Ocean Atlas. 2009 See http://www.nodc.noaa.gov/OC5/WOA09/pr_woa09.html.
85. Pearson PN, Premec-Fucek V, Premoli Silva S. 2006 Taxonomy, biostratigraphy, and phylogeny of Eocene *Turborotalia*. In *Atlas of Eocene planktonic foraminifera* (eds PN Pearson, RK Olsson, BT Huber, C Hemleben, WA Berggren), pp. 433–460. Cushman Foundation Special Publication No. 41. Fredericksburg, VA: Cushman Foundation.
86. Swart PK, Greer L, Rosenheim BE, Moses CS, Waite AJ, Winter A, Dodge RE, Helmle K. 2010 The ^{13}C Suess effect in scleractinian corals mirror changes in the anthropogenic CO_2 inventory of the surface oceans. *Geophys. Res. Lett.* **37**, L05604. (doi:10.1029/2009GL041397)
87. Pearson PN, Shackleton NJ, Hall MA. 1993 Stable isotope paleoecology of middle Eocene planktonic foraminifera and integrated isotope stratigraphy, DSDP Site 523, South Atlantic. *J. Foraminiferal Res.* **23**, 123–140. (doi:10.2113/gsjfr.23.2.123)
88. Wade BS, Al-Sabouni N, Hemleben C, Kroon D. 2008 Symbiont bleaching in fossil planktonic foraminifera. *Evol. Ecol.* **22**, 253–265. (doi:10.1007/s10682-007-9176-6)
89. Olsson RK, Hemleben CH. 2006 Taxonomy, biostratigraphy, and phylogeny of Eocene *Globanomalina, Planoglobanomalina* n. gen, and *Pseudohastigerina*. In *Atlas of Eocene planktonic foraminifera* (eds PN Pearson, RK Olsson, BT Huber, C Hemleben, WA Berggren), pp. 413–432. Cushman Foundation Special Publication No. 41. Fredericksburg, VA: Cushman Foundation.
90. Huber BT, Olsson RK, Pearson PN. 2006 *Taxonomy, biostratigraphy, and phylogeny of Eocene microperforate planktonic foraminifera* (*Jenkinsina, Cassigerinelloita, Chiloguembelina, Streptochilus, Zeauvigerina, Tenuitella, and Cassigerinella*) *and Problematica* (*Dipsidripella*). In *Atlas of Eocene planktonic foraminifera* (eds PN Pearson, RK Olsson, BT Huber, C Hemleben, WA Berggren), pp. 461–508. Cushman Foundation Special Publication No. 41. Fredericksburg, VA: Cushman Foundation.
91. Premoli Silva I, Wade BS, Pearson PN. 2006 Taxonomy of Globigerinatheka and Orbulinoides. In *Atlas of Eocene planktonic foraminifera* (eds PN Pearson, RK Olsson, BT Huber, C Hemleben, WA Berggren), pp. 461–508. Cushman Foundation Special Publication No. 41. Fredericksburg, VA: Cushman Foundation.
92. Wade BS. 2004 Planktonic foraminiferal biostratigraphy and mechanisms in the extinction of *Morozovella* in the late middle Eocene. *Mar. Micropaleontol.* **51**, 23–38. (doi:10.1016/j.marmicro.2003.09.001)
93. Roberts C, Tripati A. 2009 Modelled reconstructions of the oceanic carbonate system for different histories of atmospheric carbon dioxide during the last 20 Ma. *Glob. Biogeochem. Cycles* **23**, GB1011. (doi:10.1029/2008GB003310)
94. Sexton PF, Norris RD, Wilson PA, Pälike H, Westerhold T, Röhl U, Bolton CT, Gibbs S. 2011 Eocene global warming events driven by ventilation of oceanic dissolved organic carbon. *Nature* **471**, 349–352. (doi:10.1038/nature09826)
95. Kent PE, Hunt JA, Johnstone DW. 1971 *The geology and geophysics of coastal Tanzania*. Institute of Geological Sciences, Geophysical Paper, no. 6, 101 pp. London, UK: HM Stationery Office.
96. Derry LA, France-Lanord C. 1996 Neogene growth of the sedimentary organic carbon reservoir. *Paleoceanography* **11**, 267–275. (doi:10.1029/95PA03839)
97. Hayes JM, Strauss H, Kaufman AJ. 1999 The abundance of ^{13}C in marine organic matter and isotopic fractionation in the global biogeochemical cycle of carbon during the past 800 Ma. *Chem. Geol.* **161**, 103–125. (doi:10.1016/S0009-2541(99)00083-2)

98. Quillévéré F, Norris RD, Moussa I, Berggren WA. 2001 Role of photosymbiosis and biogeography in the diversification of early Paleogene acarininids (planktonic foraminifera). *Paleobiology* **27**, 311–326. (doi:10.1666/0094-8373(2001)027<0327:ETICOT>2.0.CO;2)
99. Bornemann A, Norris RD. 2007 Size-related stable isotope changes in late Cretaceous planktic foraminifera: implications for paleoecology and photosymbiosis. *Mar. Micropaleontol.* **65**, 32–42. (doi:10.1016/j.marmicro.2007.05.005)
100. François LM, Goddéris Y. 1998 Isotopic constraints on the Cenozoic evolution of the carbon cycle. *Chem. Geol.* **145**, 177–212. (doi:10.1016/S0009-2541(97)00143-5)
101. Wallmann K. 2001 Controls on the Cretaceous and Cenozoic evolution of seawater composition, atmospheric CO_2 and climate. *Geochim. Cosmochim. Acta* **65**, 3005–3025. (doi:10.1016/S0016-7037(01)00638-X)
102. Raymo ME, Ruddiman WF. 1992 Tectonic forcing of late Cenozoic climate. *Nature* **359**, 117–122. (doi:10.1038/359117a0)
103. Misra S, Froelich PN. 2012 Lithium isotope history of cenozoic seawater: changes in silicate weathering and reverse weathering. *Science* **335**, 818–823. (doi:10.1126/science.1214697)
104. Föllmi KB. 1995 160 m.y. record of marine sedimentary phosphorus burial: coupling of climate and continental weathering under greenhouse and icehouse conditions. *Geology* **23**, 503–506. (doi:10.1130/0091-7613(1995)023<0503:MYROMS>2.3.CO;2)
105. Huber M, Sloan LC. 2001 Heat transport, deep waters, and thermal gradients: coupled simulation of an Eocene greenhouse climate. *Geophys. Res. Lett.* **28**, 3481–3484. (doi:10.1029/2001GL012943)
106. Tyrrell T, Zeebe RE. 2004 History of carbonate ion concentration over the last 100 million years. *Geochim. Cosmochim. Acta* **68**, 3521–3530. (doi:10.1016/j.gca.2004.02.018)